Journal of the Serbian Society for Computational Mechanics / Vol. 19 / No. 1, 2025 / pp 210-224 / review paper
(10.24874/jsscm.2025.19.01.12)

# MECHANICS OF LUNG MICROSTRUCTURE AS A BASIS FOR LUNG MECHANICS, AND MULTISCALE-MULTIPHYSICS MODEL OF LUNG MECHANICS, AIRFLOW, BLOOD FLOW, AND DIFFUSION

**Milos Kojic[1,2*] [0000-0003-2199-5847], Ivo Vlastelica[3], Boban Stojanovic[4] [0000-0003-2901-0061], Vladimir Rankovic[5] [0000-0002-0407-6067], Akira Tsuda[6] [ 0000-0003-4542-1573]**

[1] Bioengineering Research and Development Center BioIRC Kragujevac, Kragujevac, Serbia
[2] Serbian Academy of Sciences and Arts, 11000 Belgrade, Serbia
[3] Higher Technical Education School, Cacak, Serbia, retired
[4]Faculty for Natural Sciences and Mathematics, Kragujevac, Serbia
[5]Faculty for Economics, University of Kragujevac, Kragujevac, Serbia
[6]Harvard School of Public Health, Boston, retired
**corresponding author*

## Abstract

This paper contains two parts – the first is related to the mechanics of lung microstructure, and the second is a formulation of a multiscale-multiphysics model of the lung. The second part considers the entire lung that relies on the mechanics of the microstructure and recently developed a multiscale composite finite element of the lung tissue (MSCL). The MSCL is further extended to include airflow, blood flow, and mass transport by diffusion, as a General Lung Finite Element (GLFE). The microstructural mechanics relies on the generally accepted Wilson-Bachofen model of balance between internal and external forces of the lung supporting system. Besides the stresses in the tissue, the effects of the surfactant play an important role in the alveolated microstructural system, vital for lung functioning. Our microstructural model demonstrates a geometric hysteresis within a duct. The multiscale-multiphysics model for airflow and blood flow is based on our smeared concept (Kojic Transport Model, KTM) where the subdomains within our Composite Smeared Finite Element (CSFE) represent the airway generations; and capillary, extracellular space and cells for blood flow and mass transport by blood. This computational methodology is built into our finite element code PAK.

**Keywords**: Multiscale composite finite element of the lung tissue, Kojic Transport Model, PAK finite element program

## 1. Introduction

Our computational model relies on the lung morphology. The lung airway structure is shown in Fig. 1. The air flows from the surrounding to the trachea, and further through two bronchi, smaller bronchi, and bronchioles. Small airways, of size 5mm to 0,5mm in diameter, form the bronchial tree, with classification as airway 23 generations. The smallest, the terminal bronchioles, are connected to the lung alveolar system, which consists of the alveolar ducts and sacs. The airway system is huge, with a length of around 2,400 kilometers. There are 300 to 500 million alveoli where the gas (nitrogen and oxygen) exchange occurs.

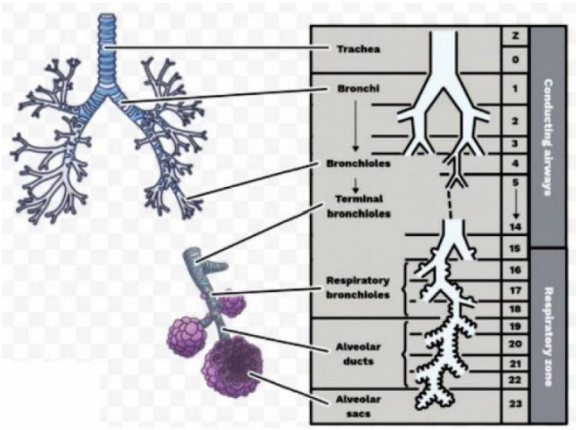


**Fig. 1** Lung morphology. The airway system starts from the trachea and ends in the lung microstructure with alveolar ducts and sacs.

Regarding the mechanics of the lung microstructure, we rely on the Wilson and Bachofen seminal work (Wilson and Bachofen, 1982a) where it was shown that the acinar airway architecture is maintained by a balance between forces pulling the alveolar duct radially inward (hoop stresses associated with tension borne in the connective tissue and smooth muscle in the alveolar entrance ring), and forces retracting the duct radially outward (primarily associated with alveolar septal surface tension at the air-liquid interface, but which may also include septal tissue tension). The microstructural model of Weibel (1986) is shown in Fig. 2 where we have a duct with the internal system of fibers which is stretched by the connection with the external system.

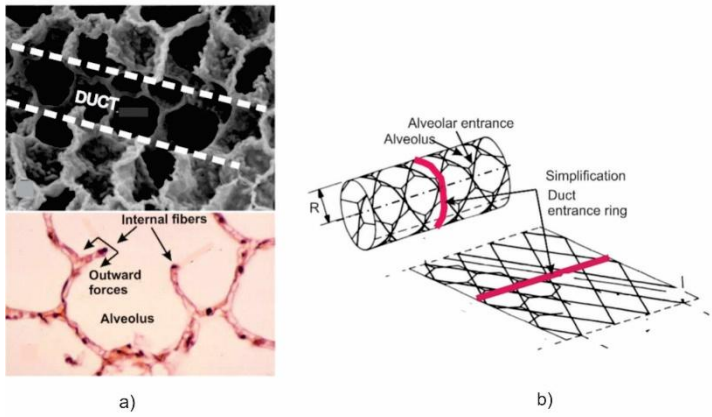


**Fig. 2** Microstructural model of Weibel (1986). a) Scanning electron micrographs of a rabbit lung - duct and alveoli with forces acting on the internal fibers. b) Fibers and alveoli in the duct, according to (Wilson and Bachofen 1982a), and the duct entrance ring as simplification used in our model. (according to Kojic, 2020).

Another duct model, important for the insight into forces within the microstructure, is shown in Fig. 3. A schematic of the duct model is displayed in Fig. 3a, while forces are shown in Fig. 3b, according to (Greaves et al. 2010). It is important to notice that the forces produced by the deformation of external tissue and surfactant ( $F_{At}^{ext}$ and $F_{A\gamma}^{ext}$ ), and by alveolar septa and surfactant ( $F_{Bt}^{\text{int}}$ and $F_{B\gamma}^{\text{int}}$ ), are acting in parallel. On the other hand, $F_{Bt}^{\text{int}}$ and $F_{B\gamma}^{\text{int}}$ forces, and force in the tissue of rings ( $F_{Ct}^{\text{int}}$ ), act as forces in series. Practically, forces ( $F_{At}^{ext}$ and $F_{A\gamma}^{ext}$ ) vs. ( $F_{Bt}^{\text{int}}$ and $F_{B\gamma}^{\text{int}}$ ) are in balance, stretching the alveolar septa tissue.

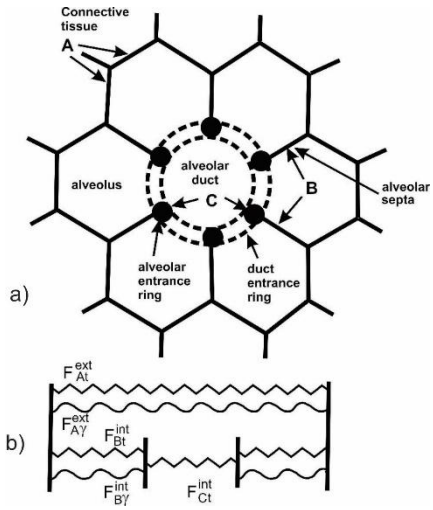


**Fig. 3.** Alveolar duct model according to Greaves et al. (2010). a) Schematic of the duct structure which includes external tissue (A) connected to alveoli, with alveolar septa (B) and entrance rings, and duct entrance ring (C); b) Forces generated by structural deformation: $F_{At}^{ext}$ and $F_{A\gamma}^{ext}$ - external connective tissue and surfactant, $F_{Bt}^{\text{int}}$ and $F_{B\gamma}^{\text{int}}$ - alveolar tissue and surfactant, and $F_{Ct}^{\text{int}}$ - alveolar and entrance rings. (according to Kojic, 2020)

Deformation of the lung internal geometry induces a change in the volume of the air space and air pressure distribution within the lung, which altogether produces the airflow deep in the lung. The airflow is conditioned by the microstructure deformation. Coupling mechanical deformation with airflow is the ultimate goal of modeling a lung.

In the next section, we shortly present our model of the mechanics of the microstructure to demonstrate a geometric hysteresis deep in the lung that affects the airflow and physical mixing important for gas exchange. Then, in the next section, a multiscale-multiphysics model of the lung is formulated according to our recent studies.

## 1. A mechanical model of the duct

The model of the alveolar duct is shown in Fig. 4, according to (Kojic, et al., 2011). The model consists of alveolar septa and entrance rings which deform due to radial cyclic displacement of the outer boundary, as schematically shown in the figure. The entire tissue is covered by a surfactant. The alveolar septa are modeled by an axisymmetric membrane, while 1D axisymmetric finite elements are used for the rings. It is assumed that the ring tissue consists of muscle tissue with hysteretic characteristics (Fig. 5c), and connective tissue without hysteresis (Fig. 5a); the volumetric ratio between the muscle and connective tissue is denoted by *m*. Material model for the alveolar septa is represented by two curves – one according to uniaxial loading, and another corresponding to biaxial loading (Fig. 5b). The model for surfactant is shown in Fig. 5d, by a hysteretic curve which relates the area ratio and surface tension.

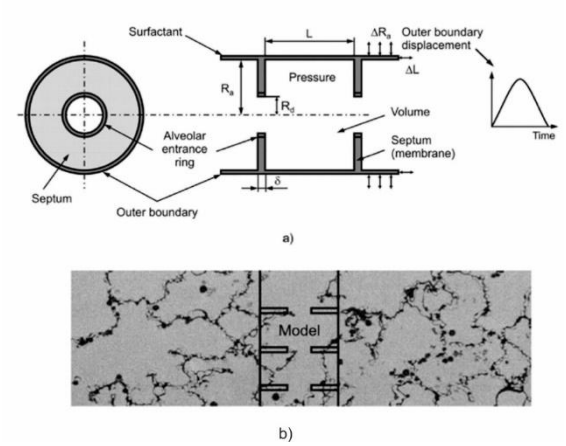


**Fig. 4** a) Duct model for the FE analysis. b) Morfology of the lung lveolar space according to (Gill, et al., 1979) and schematics of the computational model. (according to (Kojic, et al., 2011).

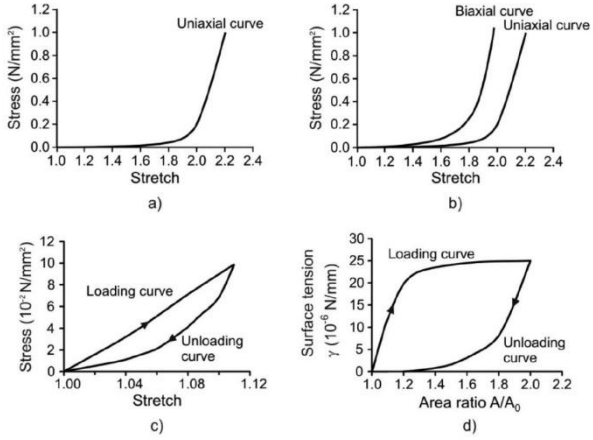


**Fig. 5.** Material models used in the FE model of the duct. a) Model of the connective tissue within the alveolar ring. b) Biaxial model for the alveolar septa. c) Muscle model for the alveolar ring. d) Model for surfactant. (according to Kojic, et al., 2011)

It was found that the ratio of the internal surface and volume of the space bounded by two alveolar septa and external boundary, has a hysteretic character, which is termed geometrical hysteresis, Fig. 6. This finding is important to understanding the physiological conditions leading to the airflow patterns that enhance gas exchange in the lung. Detailed description of the model and computational results are given in our reference (Kojic, et al., 2011).

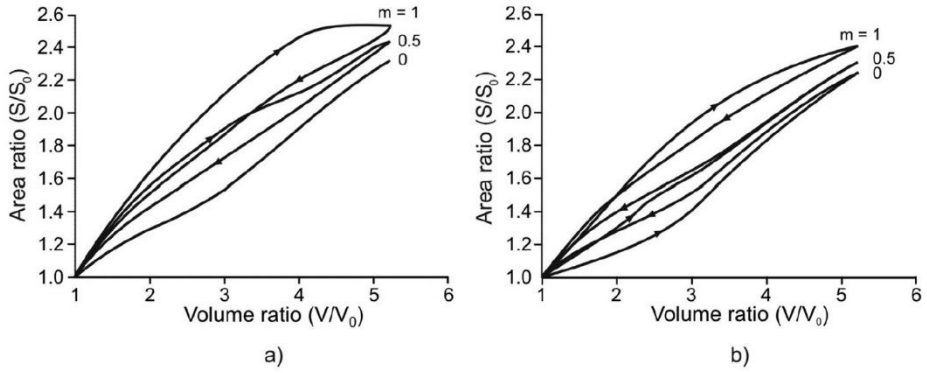


**Fig. 6** Geometric hysteresis in the alveolar space within the lung. Relations between volume and surface of the space bounded by two alveolar septa and external boundary; *m* is the ratio of muscle and connective tissue volumes within the entrance ring. (according to Kojic, et al., 2011).

## 2. Multiscale-multiphysics lung model

In this section, we present a multiscale-multiphysics model for the lung which includes mechanics, airflow, blood flow, and diffusion. The model represents a summary of our papers (Kojic, 2020) and (Kojic, 2023), with the addition of the formulation for blood flow.

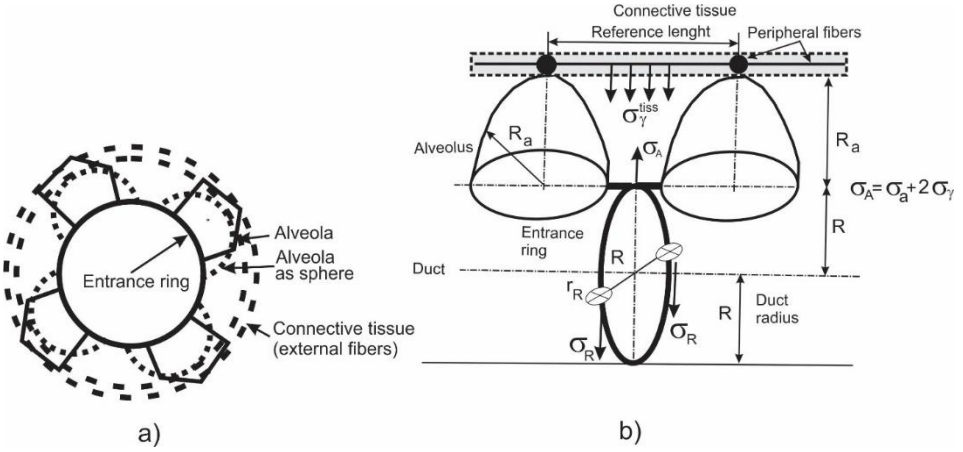


**Fig. 7** Mechanical model of the duct structure with geometry and stresses. a) Axial view; b) Axonometric view. (according to Kojic,2023)

Regarding mechanics, we use the above model in Fig. 4a and extend it to include alveoli around the circular rings as shown in Fig. 7a and assume a cylindrical external surface with connective tissue according to Fig. 7a,b. As in section 2, we assume that all solid surfaces (excluding the entrance rings) are covered by surfactant. Deformation of the internal structure occurs under the condition that forces at the ring cross-section (with stresses $\sigma_R$) and radial forces according to the stress $\sigma_A$, are in balance during the radial displacements of the external tissue. Hence, the balance equation can be written as,

$$2r_R^2\left[m\sigma_{mus}+(1-m)\sigma_{ct}\right]=R_a\delta_a n_R\left(\sigma_a+2\sigma_{a\gamma}\right) \tag{1}$$

where $r_R$ and $R_a$ are radii of the ring and alveoli (alveoli are represented as semispheres), respectively; $\delta_a$ is the alveolar thickness; $n_R$ is the number of alveoli belonging to one ring; $\sigma_a$ and $\sigma_{a\gamma}$ are the stresses within the alveolar tissue and due to surfactant, respectively; and $\sigma_{mus}$ and $\sigma_{ct}$ are the stresses in the muscle fraction and connective tissue fraction of the ring.

The stress $\sigma_\gamma^{tiss}$ acting on the external connective tissue can be expressed by the following relation.

$$\sigma_\gamma^{tiss}=n_R\frac{\left(\sigma_a+2\sigma_{a\gamma}\right)\delta_a}{2\left(R+R_a\right)} \tag{2}$$

Additionally, the stress coming from the surfactant covering the external duct surface can be expressed as

$$\sigma_{atissue}^{\gamma}=2\frac{r_{Va}}{1-r_{Va}}\frac{\gamma}{\left(R+R_a\right)} \tag{3}$$

where $r_{Va}$ is the air volumetric fraction. We can now formulate a multiscale-multiphysics finite element for the lung - a General Lung Finite Element (GLFE), shown in Fig.8. This element represents an extension of the previous finite element for lung mechanics (MSCL), (Kojic, 2020).

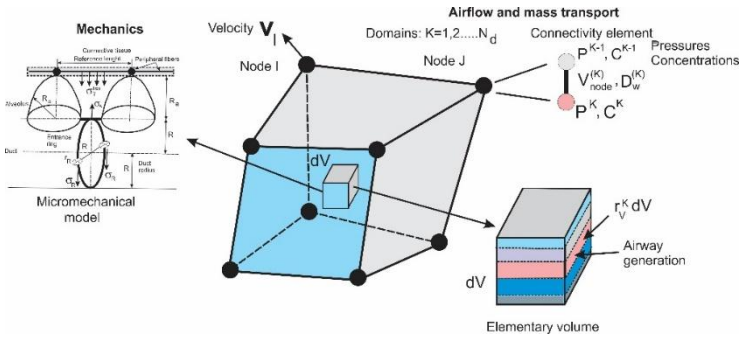


**Fig. 8** General finite element for lung (GLFE) as a multiscale-multiphysic finite element which includes mechanics, airflow, and mass transport. (according to Kojic, 2023)

We further give details on mechanics, followed by airflow, blood flow, and mass transport.

**Mechanics.** The balance equation for a finite element has a standard form (Kojic et al., 2022).

$$\left(\frac{1}{\Delta t}\mathbf{M}+\mathbf{K}\right)^{(i-1)}\Delta\mathbf{V}^{(i)}=\mathbf{F}^{ext(i-1)}+\mathbf{F}_V^{(i-1)}-\mathbf{F}^{\text{int}(i-1)}+\frac{1}{\Delta t}\mathbf{M}^{(i-1)}\mathbf{V}^t \tag{4}$$

This equation corresponds to a time step $\Delta t$ and equilibrium iteration $i$. The notation in this equation is as follows: $\mathbf{M}$ and $\mathbf{K}$ are mass and stiffness matrices**,** $\mathbf{V}$ are nodal velocities, $\mathbf{F}^{\text{ext}}$, $\mathbf{F}_V$, and $\mathbf{F}^{\text{int}}$ are external, volumetric, and internal forces; and $\mathbf{V}^{\text{t}}$ is the velocity at the start of a time step. The expressions for the matrices and nodal vectors are given elsewhere (e.g. Kojic et al., 2022). The difference with respect to the standard FE formulations is that the volumetric integration is performed over the volumetric fraction of the domain, for example, for the external connective tissue we have

$$\mathbf{F}^{\text{int}(i-1)}=\int_V r_V^{tiss}\mathbf{B}_L^{T(i-1)}\boldsymbol{\sigma}^{(i-1)}dV \tag{5}$$

Here, $r_V^{tiss}$ is the tissue volumetric fraction, which can be expressed in terms of the air volumetric fraction as $r_V^{tiss}= 1-r_{Va}$, $\mathbf{B}_L$ is the strain-displacement matrix, and $\boldsymbol{\sigma}$ is the stress tensor within the connective tissue. Following the above description, the stress in (5) can be expressed as

$$\sigma_{ii}=\sigma_{ii}^{tiss}+\sigma_{\gamma}^{tiss}+\sigma_{atissue}^{\gamma},\quad ii=1,2,3,\ no\ sum\ on\ i \tag{6}$$

where $\sigma_{ii}^{tiss}$ is stress due to the deformation of external connective tissue.

In order to solve the balance equation (1), we use the following geometrical relations related to the duct radius $R$:

$$R_{\min}=R_o,\quad R_{\max}=\lambda R_0 \tag{7}$$

Then, using a simple bisection procedure for the radius range $R_{min}$ -$R_{max}$, we follow the computational steps:

- Current R
- Compute $\lambda_R= R/R_0$ and stress in the ring from $\lambda_R$ and constitutive curves in Fig. 5a,c.
- Compute stretch of alveolus $\lambda_a$ from $R_a= \lambda\ (R_0+R_{a0})-R$, $\lambda_a= R_a/R_{a0}$ and stress $\sigma_a$ form constitutive curves in Fig. 5b.
- Alveolar area ratio is $\lambda_{a\gamma}=R_a^2/R_{a0}^2$ and surface tension $\gamma$ compute using the constitutive curve in Fig. 5d, so that we have the stress $\sigma_{a\gamma}=\gamma/\delta_a$ .
- Compute the external surface area ratio $\lambda_{ext\gamma}=\left(R+R_a\right)^2/\left(R_0+R_{a0}\right)^2$ , surface tension according to the constitutive curve in Fig. 5d, and external stress $\sigma_{atissue}^{\gamma}$ from (3)

- Update the air volumetric fraction as $r_{Va} = \eta r_{Va0}$, where

$$\eta = \frac{\pi \left(R + R_a\right)^2 L_{duct}}{\pi \left(R_0 + R_{a0}\right)^2 L_{duct0}} = \lambda \frac{\left(R + R_a\right)^2}{\left(R_0 + R_{a0}\right)^2} = \lambda^3 \tag{8}$$

Here, $L_{duct}$ and $L_{duct0}$, are current and initial duct lengths, and with the isotropy assumption $L_{duct} / L_{duct0} = \lambda$.

**Airflow.** We have implemented two models for the incompressible fluid flow in blood vessels: a) 3D or axisymmetric 2D Navier-Stokes equations, or b) the approximate 1D Hagen-Poiseuille model. In our mixed formulation, the finite element balance equations for the Navier-Stokes model, the balance incremental-iterative equations for a finite element can be written in the form (e.g. Kojic et al., 2022),

$$\begin{bmatrix} \frac{1}{\Delta t}\mathbf{M} + \tilde{\mathbf{K}}_{vv}^{(i-1)} & \mathbf{K}_{vp} \\ \mathbf{K}_{vp}^T & \mathbf{0} \end{bmatrix} \begin{Bmatrix} \Delta \mathbf{V}^{(i)} \\ \Delta \mathbf{P}^{(i)} \end{Bmatrix} = \begin{Bmatrix} \mathbf{F}_{ext}^{(i-1)} \\ \mathbf{0} \end{Bmatrix} - \begin{bmatrix} \frac{1}{\Delta t}\mathbf{M} + \mathbf{K}_{vv}^{(i-1)} & \mathbf{K}_{vp} \\ \mathbf{K}_{vp}^T & \mathbf{0} \end{bmatrix} \begin{Bmatrix} \mathbf{V}^{(i-1)} \\ \mathbf{P}^{(i-1)} \end{Bmatrix} + \begin{Bmatrix} \frac{1}{\Delta t}\mathbf{M}\mathbf{V}^t \\ \mathbf{0} \end{Bmatrix} \tag{9}$$

The detailed description of the element matrices in the reference (Kojic et al. 2022). The nodal variables are velocities **V** and pressures **P**. The nodal variable in the case the Hagen-Poiseuille flow model is the fluid pressure only, and the FE balance equations are

$$\mathbf{K}_p^{(i-1)} \Delta \mathbf{P}^{(i)} = \mathbf{Q}_p^{ext(i-1)} - \mathbf{K}_p^{(i-1)} \mathbf{P}^{(i-1)} \tag{10}$$

Here, $\boldsymbol{Q}_p^{ext}$ is the external nodal fluid flux (which cancels at the internal FE nodes). The 2x2 transport matrix is

$$K_{p11} = K_{p22} = -K_{p12} = -K_{p21} = \frac{\pi d^4}{128\mu} \tag{11}$$

where $d$ is the airway diameter and $\mu$ is air viscosity.

We implement the Kojic Transport Model (KTM), (Kojic et al., 2022) as the equivalent continuum model for small airways within the lung parenchyma. The flow domains within our composite smeared finite element consist of the selected groups of small airways within the airway generation tree. The domains are specified according to the size of the airways. The 3D continuum balance equations have the form (10), with the equivalent Darcy transport tensor,

$$k_{Dij} = \frac{\pi}{128\mu A_{tot}} \sum_J d_J^4 \ell_{Ji} \ell_{Jj} \tag{12}$$

where $d_J$ are airway diameters, and $l_{Ji}$ are directional cosines of small airways in the vicinity of the considered point $J$ within the parenchyma. The connection between 1D (pipe) elements when the pipe elements have permeable walls, or in the case of branching into smaller airways, is achieved by the corresponding 1D connectivity elements. The connectivity elements are also used for the coupling between the domains of the composite finite elements, according

to the KTM methodology. The 2-node transport matrix for the connectivity elements has the form (11), so that, for a node *J*, we have

$$K_{J11} = K_{J22} = -K_{J12} = -K_{J21} = h_{pJ} V_J \tag{13}$$

Here, we have that $h_{pJ}$ is the permeability (resistance) coefficient, and $V_J$ is the volume of the continuum belonging to the node. We use the permeability coefficient to be proportional to the mean value of the diagonal terms of the transport tensor and inversely proportional to the airway diameter at the node. We include the alveolar sacs in the model in the form of a source within the last domain of the KTM, as

$$q_V = r_{Vsac} dV / dt \tag{14}$$

where $r_{Vsac}$ is the sac volumetric fraction, while *dV/dt* represents the rate of the volume change evaluated in the mechanical model (pass 1 in the computational procedure described below).

**Blood flow.** The model for blood flow is analogous to the airflow. For large blood vessels, equation (9) is applicable, with the appropriate material parameters – density and viscous coefficient. Regarding the flow within capillaries, we can apply the KTM, where the capillary volumetric fraction can be expressed as

$$r_V^{cap} = r_V^{rcap} \left(1 - r_{Va}\right) \tag{15}$$

where $r_V^{rcap}$ is capillary density with respect to lung tissue volume.

The Dracy tensor has the form (12). The flow within extracellular space occurs according to equation (10) – for 3D conditions and with the Darcy coefficient of the extracellular space (Kojic, et al. 2022); the volumetric fraction is

$$r_V^{ex} = \left(1 - r_V^{rcap} - r_V^{rcell}\right)\left(1 - r_{Va}\right) \tag{16}$$

where $r_V^{rcell}$ is cell density relative to the lung tissue. The connectivity elements are as in the case of the air, with using the appropriate hydraulic coefficients. Also, instead of the volume $V_J$, the area $A_J$ belonging to the node must be used: $A_J = r_{AV} V_J$, where $r_{AV}$ is the area-to-volume ratio of the capillary.

The blood flow model which includes large vessels, capillaries, and extracellular space is illustrated in Fig. 10.

**Mass Transport (Diffusion).** Particulate (molecular) transport within the air is modeled as a diffusion with convection. The mass balance equation for a finite element and a domain K can be written as (Kojic et al., 2022)

$$\left(\frac{1}{\Delta t}\mathbf{M} + \mathbf{K} + \mathbf{K}^v\right)^{K(i-1)} \Delta \mathbf{C}^{K(i)} = \mathbf{Q}^{KS(i-1)} + \mathbf{Q}^{KV(i)} - \left(\frac{1}{\Delta t}\mathbf{M} + \mathbf{K} + \mathbf{K}^v\right)^{K(i-1)} \mathbf{C}^{K(i-1)} + \frac{1}{\Delta t}\mathbf{M}^K \mathbf{C}^{Kt} \tag{17}$$

The expressions for the matrices are given in (Kojic et al. 2022), and **C** is the nodal concentration 1D matrix. This form of the balance equation applies to large airways and the Navier-Stokes equations. Additionally, we here include the alveolar sacs as a domain according to their diffusive characteristics. The air velocities are included in the balance equations through the convection matrix $\mathbf{K}^{v}$, with the velocities obtained from the airflow. The diffusion tensor for the parenchyma subdomains has the form analogous to (12), i.e.,

$$D_{ij} = \frac{1}{A_{tot}} \sum_{J} A_J D_J \ell_{Ji} \ell_{Jj} \tag{18}$$

where $A_J$ and $D_J$ are cross-sectional areas and diffusion coefficients, respectively. The connectivity elements are defined as in the case of airflow, with diffusion coefficients to be used in (13) instead of the hydraulic resistance coefficients $h_{pJ}$.

We can also consider diffusion within blood, which is governed by equations analogous to those within the air. Here, we need to use the appropriate diffusion coefficients within capillaries, extracellular space, and cells (Kojic et al.,2022).

In this section, we summarize the concept of the entire lung model by using the above description of finite elements for mechanics, airflow, and diffusion. This general lung model is shown in Fig. 9. Note that large airways have the same equation numbers for velocities with the surrounding continuum. In the case of airflow and diffusion, large airways are not connected to the surrounding continuum, while smaller airways modeled by 1D pipe elements may have a connection (connectivity elements) with the first domain of the composite smeared 3D finite elements (GLFEs).

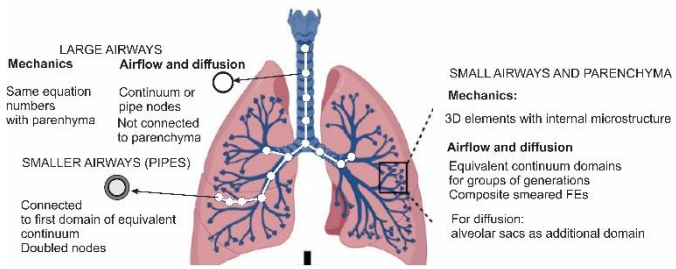


**Fig. 9.** Finite element model for the entire lung. The model includes mechanics, airflow, and diffusion. Connectivities between domains are shown in the model. (according to Kojic, 2023).

These finite elements and computational procedure according to details given in Fig.9 are built in our finite element code PAK-BIO, a modulus of PAK (Kojic et al., 2024). The following computational steps (passes) are implemented into the code for each time step: (according to Kojic, 2023)

- Pass 1 – **Mechanics**. Velocities and displacements of the solid are determined. In the case of blood flow, the time step corresponding to blood should be used (which is smaller than needed for the airflow).

- Pass 2 – **Airflow**. Geometry and velocity field of the solid are used from Pass 1. Airflow is determined by computing the pressure field. In the case of coupling 2D or 3D models with the pipe 1D elements, two separate FE meshes are generated and two systems of equations are successively solved within iterations until convergence is reached for both systems.

- Pass 3 –**Diffusion**. Geometry and velocity field of the air are used from passes 1 and 2. In the case of coupling a 2D or 3D model with the pipe elements, one finite element mesh is generated and one system of equations is solved until convergence criteria are satisfied.

In case of diffusion within the blood, we need a pass 4 using large blood vessels and the same mesh in the parenchyma (Fig. 10) and the corresponding time step. This model provides a basis for extension to include gas exchange.

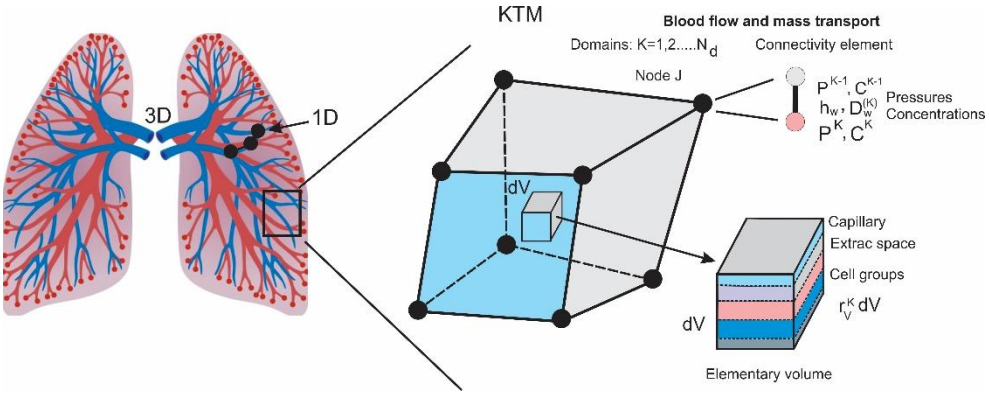


**Fig. 10.** Computational model for blood flow that includes 3D Navier-Stokes, 1D Hagen-Poisseule, and KTM formulations.

## 3. Examples

Here, we present two simple examples, according to (Kojic, 2023), to illustrate the methodology built into our code PAK. They demonstrate the main characteristics of our theoretical formulations and characteristics that are in agreement with the mechanical behavior of the lung parenchyma, which is dominant for lung function. We put in quotes the entire section, since it is borrowed from the reference (Kojic, 2023).

### *4.1 Three-axial stretch*

One element is subjected to high stretches in all directions, as shown in Fig. 11. The stretch increases up to the value of displacements 1 [mm] and then decreases to zero, simulating a lung cycle, as shown in the figure; hence doubling the element size. We impose these high stretching to emphasize the character of the deformation of microstructural elements. The goal of the example is to gain insight into these deformations which are of vital importance for lung function (Kojic et al., 2011). Regarding the microstructural data, we have used (lengths in

[mm]): entrance ring radius $R$= 0.1, entrance ring cross-section radius $r_R$ =0.05, alveolus radius $R_a$= 0.2, alveolus thickness $\delta_a$= 0.01; ratio muscle/connective tissue in entrance ring $m$=0.2; radial alveolar density $n_R$=6.

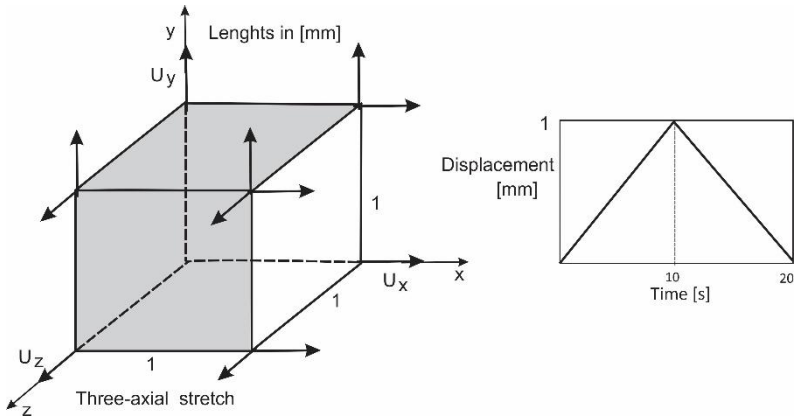


**Fig.11.** Three-axial stretch of the General Lung Finite Element (GLFE). (according to Kojic, 2023).

Figure. 12 shows a change of the duct volume (relative to the initial) and internal ring size over a cycle. It can be seen that the volume changes nonlinearly without hysteresis since the change of the external boundary does not have hysteretic character (Fig. 11). On the other hand, due to the hysteresis of surfactant and internal ring (Figs. 5c,d) the internal ring radius displays hysteresis – with the size larger in the unloading (lung expiration), Fig.12b.

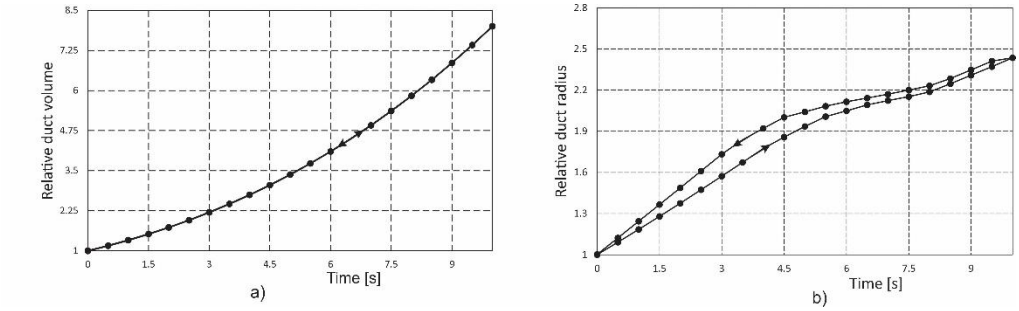


**Fig.12.** Change of the duct volume a), and internal ring size b), over a lung cycle (time during unloading-expiation goes from 10 to 0). (according to Kojic, 2023)

*4.2 Example 2 – Coupling between large and small vessels*

In a simple example shown in Fig. 13, we illustrate the coupling between two domains according to the procedure following from the presentation here and in (Kojic, 2023). As shown in Fig. 13, we consider a fluid domain (3D or axisymmetric, boundary elements 1-5) – on the left, coupled to four 1D pipe elements with boundary nodes 3,4,19,22. The parenchyma is

modeled by two 3D GLFEs. The length of each fluid element is 2 [mm] while the length of each of the GLFEs is equal to 1 [mm]. Axial symmetry is assumed for fluid, with an approximately parabolic profile at the entering left surface, and velocity at the symmetry line equal to 1 [mm/s]. It is taken that fluid density is equal to 0.001 [g/mm$^3$] and viscosity 0.001 [Pas]. Constant concentration is prescribed at the left entrance equal to 1 [M]. It is assumed that the prescribed velocity increases linearly during the inspiration period of 10s and linearly decreases to zero at time 20s (time function shown in Fig. 11); the diffusion coefficient is D=10 [mm$^2$s$^{-1}$].

The fluid domain is connected to the parenchyma through four pipes with boundary nodes 3,4,19,22. The diameters of pipes are taken to be 2 [mm]. We have used a very small elasticity modulus for pipes (E=0.001Pa) to emphasize the mechanical response of the lung parenchyma. It can be seen that connectivity elements between pipes and GLFEs are 3-11, 4-9, 19-1,.., 24-14. The hydraulic proportionality coefficient is 0.7. Pressure and concentration at the pipe end nodes are imposed to be zero. It is adopted that there are 4 groups of small airways (generations) with diameters (in [mm]): 2, 1.5. 1, 0.5, and equal volumetric fractions $r_V$=0.1. The last domain represents the alveolar sacs. The solid is subjected to three-axial uniform mechanical loads, with fixed left and back surfaces with sliding conditions on these surfaces. Maximum force at nodes is 3x10$^{-4}$ [N] for nodes at edges and 6x10$^{-4}$ [N] for other nodes.

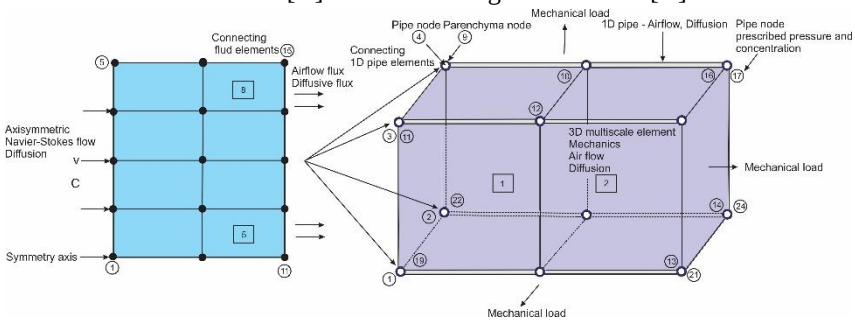


**Fig.13.** Two models coupled. 3D or axisymmetric fluid domain (left) coupled to 1D (pipe) model within a 3D parenchyma model (3D GLFE elements). Boundary fluid elements 5-8 are connected to boundary pipe nodes 3,4,19,22. (according to Kojic, 2023).

The goal of this example is to show a mechanical hysteretic character of the overall solid continuum and to illustrate airflow from the continuum fluid to the pipe structure. Fig. 14 shows the normal displacement of the right surface over a cycle, with a hysteresis. In Fig. 15, the pressures within the pipe and subdomains are shown.. Pressures increase linearly at inspiration and then decrease during expiration.

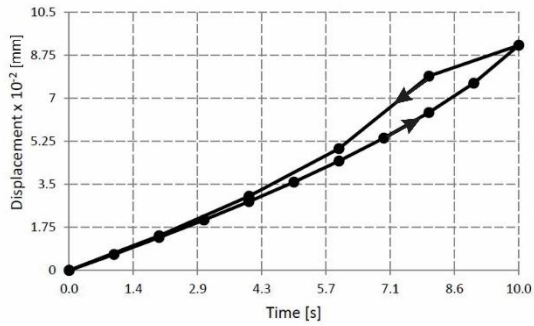


**Fig.14.** Displacement of the right solid surface over a cycle (time during unloading goes from 10 to 0). (according to Kojic, 2023).

There is no hysteresis in pressure. It can be seen that pressure decreases over domains, with the decrease becoming smaller from the first to the last domain.

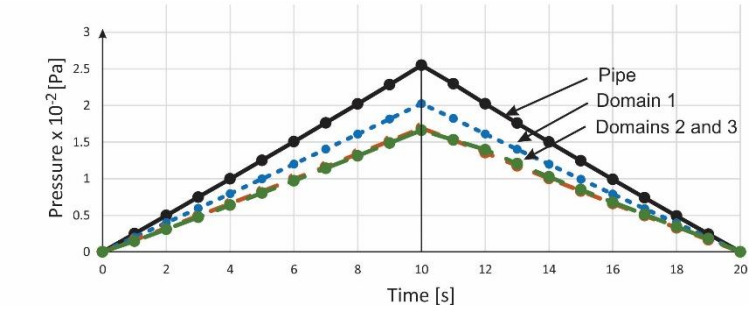


**Fig.15.** Pressure within pipe connections with fluid and for a point within small airway domains over time. There is no notable hysteresis over the cycle. (according to Kojic, 2023).

## 4. Conclusions

We have briefly summarized our research, which started in 2001. and ending in 2024. The formulations and implementation into the PAK (Kojic et al., 2024) code belong mainly to the first author, but they were supported by important contributions of the other authors.

This development represents a solid basis for further modeling of the real physiological conditions and implementations, supported by modern methodologies in imaging, model generation, and the today attractive artificial intelligence. We believe that this methodology and software will serve as a useful tool in the medical practice.

**Acknowledgments:** The author acknowledges continuous support from the City of Kragujevac, Serbia, and the Ministry for Sciences and Education of Serbia; to the Serbian Academy of Sciences and Arts, Grant F-134; to Harvard School of Public Health; and to HoustonMethodist Research Institute. The authors are thankful to Dr. James P. Butler, Harvard School of Public Health for earlier joint work in this field.

## References

Greaves I. A., Hildebrandt J., Hoppin Jr. F. G. (2010), Micromechanics of the Lung, *Handbook of Physiology – Chapter 14 The Respiratory System*, American Physiological Society.

Kojic, M., Butler, J. P. , Vlastelica I., Stojanovic,B., Rankovic,V., Tsuda,A., Geometric hysteresis of alveolated ductal architecture, ASME J. Biomechanics, Vol. 133 / 111005-1-11, 2011.

Kojic, M., Slavkovic,R. Zivkovic, M., Grujovic, N., Filipovic, N., Miloseevic, M., Rakic, R., Dunic, V., 2024, PAK – Finite Element Program for Engineering and Bioengineering; PAK-BIO - Mudule for Bioengineering, University of Kragujevac, Bioengineering R&D Center BIOIRC, Kragujevac, Serbia.

Kojic,M. 2020, Multiscale composite 3d finite element for lung mechanics, J. Serbian Soc. Comp. Mech. 14(1) , 1-11.

Kojic, M., Milosevic, M., Ziemys,A., Computational Models in Biomedical Engineering - Finite Element Models Based on Smeared Physical Fields: Theory, Solutions, and Software, Elsevier, 2022.

Kojic,M. 2023, A multiscale multiphysics finite element for lung, Journal of the Serbian Society for Computational Mechanics / Vol. 17 / No. 2, 1-15.

Weibel, E. R., 1986, Functional Morphology of Lung Parenchyma, Handbook of Physiology, The Respiratory System, A. P. Fishman, ed., Sec. 3, Vol. III, Chap. 8, American Physiological Society, Bethesda, MD, pp. 89–111.

Weibel, E. R., and Gil, J., 1977, Alveolar Structure-Function Relationships, Bioengineering Aspects of the Lung, J. B. West, ed., Marcel Dekker, New York.

Wilson T. A., and Bachofen H., 1982a, A Model for Mechanical Structure of Alveolar Duct, *J. Appl. Physiol., Respir. Environ. Exercise Physiol.*, 52(4), 1064–1070.

Wilson, T. A., 1982b, Surface Tension-Surface Area Curves Calculated from Pressure-Volume Loops, *J. Appl. Physiol.: Respir. Environ. Exercise. Physiol.*, 53(6), 1512–1520.